Conversion Syzygium oleana leaves biomass waste to porous activated carbon nanosheet for boosting supercapacitor performances

by Rika Taslim

Submission date: 07-Dec-2020 10:28AM (UTC+0700)
Submission ID: 1466935865
File name: 1-s2.0-S2238785420317774-main.pdf (1.67M)
Word count: 5843
Character count: 31913

J MATER RES TECHNOL. 2020;9(xx):13332–13340

Available online at www.sciencedirect.com

jmr&t Journal of Materials Research and Technology

https://www.journals.elsevier.com/journal-of-materials-research-and-technology

Original Article

Conversion *Syzygium oleana* leaves biomass waste to porous activated carbon nanosheet for boosting supercapacitor performances

Erman Taer[a,*], *Apriwandi Apriwandi*[a], *Rika Taslim*[b], *Agustino Agutino*[a], *Deris Afdal Yusra*[a]

[a] *Department of Physics, University of Riau, 28293 Simpang Baru, Riau, Indonesia*

[b] *Department of Industrial Engineering, State Islamic University of Sultan Syarif Kasim, 28293 Simpang Baru, Riau, Indonesia*

ARTICLE INFO

Article history:
Received 27 July 2020
Accepted 10 September 2020

Keywords:
Electric double layer capacitor
One-Stage pyrolysis
Nanosheet
Porous carbon
Syzygium oleana

ABSTRACT

The porous activated carbon nanosheet derived from *Syzygium oleana* leaves biomass was prepared by one-stage integrated pyrolysis through both carbonization and physical activation for supercapacitor electrode as energy storage application. Carbonization was performed in three different temperatures, including 500 °C, 600 °C, and 700 °C. The 1 M potassium hydroxide was selected to produce activated carbon progressively. Importantly, the surface morphology and the sample were characterized by Scanning electron microscopy at a voltage of 15 kV and nitrogen adsorption/desorption at a temperature of 77 K. The results showed a like-flower nanosheets structure decorated by nanofiber increases the surface area of activated carbon from 216 $m^2\ g^{-1}$ to 1218 $m^2\ g^{-1}$ with tuneable well confirmed mesopores sizes. Degree of crystallinity and chemical composition also were characterized by using X-ray diffraction and Energy dispersive spectroscopy. Furthermore, electrochemical measurements had the best performances with a high specific capacitance of 188 F g^{-1} at two-electrode system with a scan rate of 1 mV s^{-1}.

1. Introduction

Since their entrance in the industry 4.0 era, nanomaterials and nanotechnology have become one of the most popular areas of interest among researchers. Different nanomaterials with various structures, including 0D, 1D, 2D, and 3D nanostructures were created to develop practical applications [1]. Carbon structured nanomaterials are often preferred in developing nanotechnology because of their lightweight, high strength and high conductivity [2]. Several applications use nanomaterials and nanotechnology, including electrochemical sensing [3], imaging cells [4], catalysis [5], energy storage [6], increasing the capacitive performance of supercapacitors [7], electrocatalysis, electrochemical catalysis [8], sensing DNA [9], and hydrogen sensor [10]. The use of nanomaterials as an electrode material to enhance supercapacitors is proliferating. They are mainly used because of the provision of large pores, high sur-

* *Corresponding authors.*
E-mails: erman.taer@lecturer.unri.ac.id (E. Taer), apriwandi95@gmail.com (A. Apriwandi), rikataslim@gmail.com (R. Taslim), agustino@student.unri.ac.id (A. Agutino), derisafdaly@gmail.com (D.A. Yusra).

https://doi.org/10.1016/j.jmrt.2020.09.049

face area, well-defined diverse structures, efficient electron transportation, and unique electric charge transport features [11,12].

However, not all nanomaterial structures are obtained easily and provide excellent properties to improve supercapacitor performance. Different nanomaterial structures exhibit different electrochemical activities, which is vital for supercapacitor electrodes, including EDLC and pseudocapacitors [13]. The synthesis of electrodes with homogeneous, regular, high-density nanomaterial structures requires complex preparation and has relatively more expensive production costs, including materials from carbon, metal oxides, metal sulfides, metal nitrides, conduction polymers, and nanocomposites [14,15].

Graphene oxide and silicon oxide template methods are often used to prepare 2D nanosheet structures from porous carbon with excellent supercapacitor performance [16]. Although other approaches also use post-activation and self-assembly techniques, they still have many shortcomings, such as synthetic procedures that need to be multistep. Also, the production costs are relatively expensive because they use synthetic materials, making them unfit for large scale applications and eliminating relatively complicated templates. Still, they require extra time or high energy consumption due to their chemical properties and stable hard templates. Additionally, the resulting nanosheet is relatively thick, which is not suitable for improving supercapacitor performance [7]. These obstacles are significant challenges for developing porous 2D nanosheet structures for high-performance supercapacitors with effective and efficient methods.

This study focuses on an alternative, simple, up to date, and relatively low-cost method for synthesizing porous 2D carbon nanosheets from *Syzygium oleana* leaves waste. It uses one-stage integrated pyrolysis with carbonization temperature of 500, 600, and 700 °C is the main focus to increasing the capacitive performance of supercapacitors. The various carbonization temperatures have been investigated for the main part of converting the biomass waste into porous activated carbon material. The carbonization affected the porosity development due to the potential conversion of activating reagents such as KOH or NaOH to their corresponding carbonates which could be produced activated carbon with both micro and mesoporosity depending on the carbonization temperature [17].

Syzygium oleana is a type of shrub belonging to the Myrtaceae family. It is mostly found in Indonesia as an ornamental plant often found embedded in pots on the edges of roads. Apart from being an ornamental and helping to control air pollution in the city, this plant is underutilized. It is rich in lignocellulose, which a potential raw material for activated carbon [18]. Generally, activated carbon electrodes are maintained in the form of monoliths without adhesives. Integrated one-stage pyrolysis was selected for the carbonization and physical activation process with KOH as a chemical activator agent. One-stage integrated pyrolysis allows shorter time carbon nanosheet yield and therefore can be used for large-scale nanomaterial production. *Syzygium oleana leaves* are the first pure biomass to be reported as a potential material for carbon nanosheets without the template method, composite, and the addition of other synthesis materials. The samples morphology showed that the high-density nanosheet structure was decorated nanofibers, it significantly increased the specific surface area from 216 to 1218 $m^2 g^{-1}$ and improved the high-performance of supercapacitors.

2. Materials and methods

Activated carbon made from *Syzygium oleana* leaves (ACSs) was prepared using one-stage integrated pyrolysis. The *Syzygium oleana* leaves wastes were collected from the environment of Riau University, Indonesia. Initially, the *Syzygium oleana* leaves wastes were washed and dried for 2 days at a temperature of 110 °C. Pre-carbonated leaves are dried in the room temperature to 250 °C with a periodic rate of 50 °C/30 min. Before the pyrolysis process, biomass samples were mixed with KOH in the mass ratio of KOH and carbon powder of 1:3.5. Furthermore, the carbon powder was converted into a monolith/pellet form using a hydraulic press without adhesive materials where 10 samples were tested for each monolith carbon. Pyrolysis process, including carbonization and physical activation, is performed in a one-stage integrated furnace tube. Carbonization is performed in the N_2 atmosphere at a temperature of 30 °C–289 °C with a periodic temperature rise of 1 °C min^{-1}. Pyrolysis was held for 60 min at 289 °C to remove organic and volatile compounds, as well as to decompose cellulose, hemicellulose, and lignin completely. Afterwards, the temperature was raised 3 °C min^{-1} to the maximum carbonization temperature of 500 °C, 600 °C, and 700 °C. The pyrolysis process is continued with physical activation in a CO_2 with an increase of 10 °C min^{-1} to a high temperature of 850 °C for 150 min, as shown in Fig. 1. To facilitate the results and discussion, the samples were marked with ACS500, ACS600, and ACS700. The number on the label indicates carbonization temperature, while all carbon monoliths are neutralized using distilled water.

The sample morphology was observed by scanning electron microscopy (SEM, JEOL JSM-6510 LA) at a voltage of 15 kV and X-ray diffraction (XRD) on Philip X-Pert Pro PW 3060/10 using Cu Kα radiation at an angle of 0–60°. The element content is recorded by energy dispersive spectroscopy (EDS, JEOL JSM-6510 LA) in the range of 0–20 KeV at 15 kV. The N_2 gas adsorption was obtained at liquid nitrogen temperature of 77 K using the Quantachrome TouchWin v1.2 instrument. The Brunauer-Emmett-Teller and Barrett-Joyner-Halenda method were implemented to calculate the specific surface area and pore size distribution.

The electrochemical performance of ACSs monolith electrodes was measured in two-electrode systems using the Cyclic Voltammetry (CV, Rad-Er 5841 instrument, calibrated with VersaStat II Princeton Applied Research with an error of ±6.05 %,) method. Symmetrical capacitors were assembled with two working electrodes separated by duck eggshell membranes [19]. Measurements were performed in 1 M H_2SO_4 solution. The CV was carried out from 0.0–1.0 V at different scan rates from 1 to 10 mV s^{-1}.

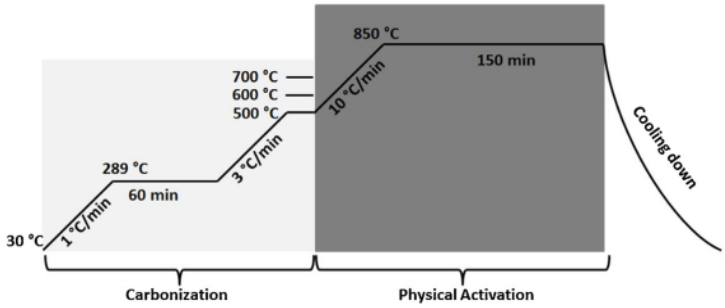

Fig. 1 – One-stage integrated pyrolysis process of ACSs samples.

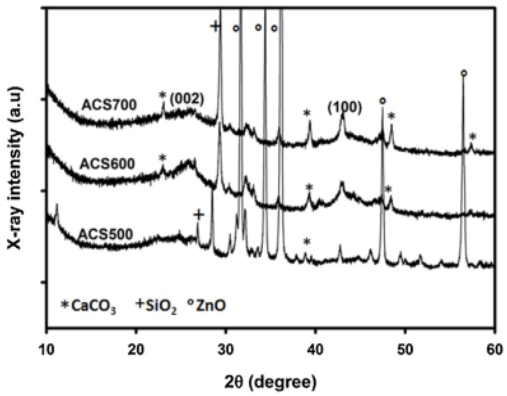

Fig. 2 – XRD pattern of ACSs samples.

3. Results and discussions

Fig. 2 shows the XRD pattern of ACSs monolith based on different carbonization temperatures of 500 °C, 600 °C, and 700 °C. There are two clear characteristic peaks around 24–26° and 43–46°. The peak centered at 24–26° is associated with the diffraction plane (002), showing an excellent amorphous structure of carbon biomass material [20]. Similarly, the peak at 43–46° corresponds to the plane (100), representing a small amount of hexagonal graphite (JCPDS No. 41-1487). This also similar found at other study with different raw materials such as durian shell [21], and *mangosteen* [22], which are shown two broad strong peaks at 2θ angles of 22–24° and 42–44°. Furthermore, the diffraction of the (002) and (100) lattice peaks of ACS700 moved to a lower angle from 26° to 24° and from 45° to 43°, indicating that the interlayer spacing of ACS700 were greater than the ACS500 and ACS600. This may have been due to the existence of vast micropores and a random combination of graphitic and chaotic stacking which expected higher specific surface area. The presence of these two peaks contributes to certain micropores levels and increases the electronic conductivity [23]. Additionally, the presence of sharp peaks is also shown in the XRD pattern, indicating the existence of crystal elements in the sample, such as $CaCO_3$ (JCPDS No. 82-1690), SiO_2 (JCPDS No. 89-1668), and ZnO (JCPDS No. 79-2205). The existence of this compound is extracted from the basic elements of *Syzygium oleana* leaves biomass. The carbonization temperature applied to the sample reduces its crystalline behavior. The carbonization temperature of 500 °C shows the crystallinity of non-carbon impurities, including $CaCO_3$, SiO_2, and ZnO, characterized by high-X-ray intensity. The increase in carbonization temperature at 600 °C and 700 °C shows that the X-ray intensity is relatively smaller, the ZnO element is correctly reduced and leaves $CaCO_3$ and SiO_2. However, the presence of ZnO contributes to the supply of diffusion ions process on the electrode surface [24]. This compound is act as pseudocapacitance behavior, increasing supercapacitor performance. This is confirmed by the cyclic voltammetry profile discussed in the next subsection.

The surface morphology of the ACSs monoliths obtained was marked by SEM micrographs, as shown in Fig. 3. This shows the morphology of the activated carbon derived from *Syzygium oleana* leaves were subjected to differences in carbonization temperatures of 500 °C, 600 °C, and 700 °C. The irregular structure of nanosheets can be observed in all SEM images. As shown in Fig. 3a, the morphology of the sample resembles irregular nanosheets with a rough surface. At greater zoom, nanosheets have fractures with tangled surfaces and small amounts of nanofibers with a diameter of 90–132 nm, as shown in Fig. 3b. The carbonization temperature of 500 °C decomposes cellulose, hemicellulose, and lignin, raising fiber even in small amounts. The high-temperature physical activation has not shown the larger pores development, though it effectively produces the structure of fractured nanosheets. These nano-scale structures effectively prevent nanosheet stacks, increase open surface area, facilitate the diffusion of electrolyte ions in sheet-to-sheet, and offer more active sites to form electric double layers [25].

As carbonization temperature raises from 500 °C to 600 °C, surface morphology changes, ACS600 appears in relatively larger forms of nanosheets, where large pores are found as shown in Fig. 3c. Additionally, the ACS600 also shows nanofibers with fiber diameters between 74–121 nm, which are also attached to the nanosheet, as shown in Fig. 3d. The appearance of SEM micrographs on ACS600 shows the temperature carbonization process of 600 °C has effectively disentangled the hemicellulose and lignin attached to the cellulose, and therefore, fibers are more dominant on the sample surface [18]. The relatively large amount of fibers allows for

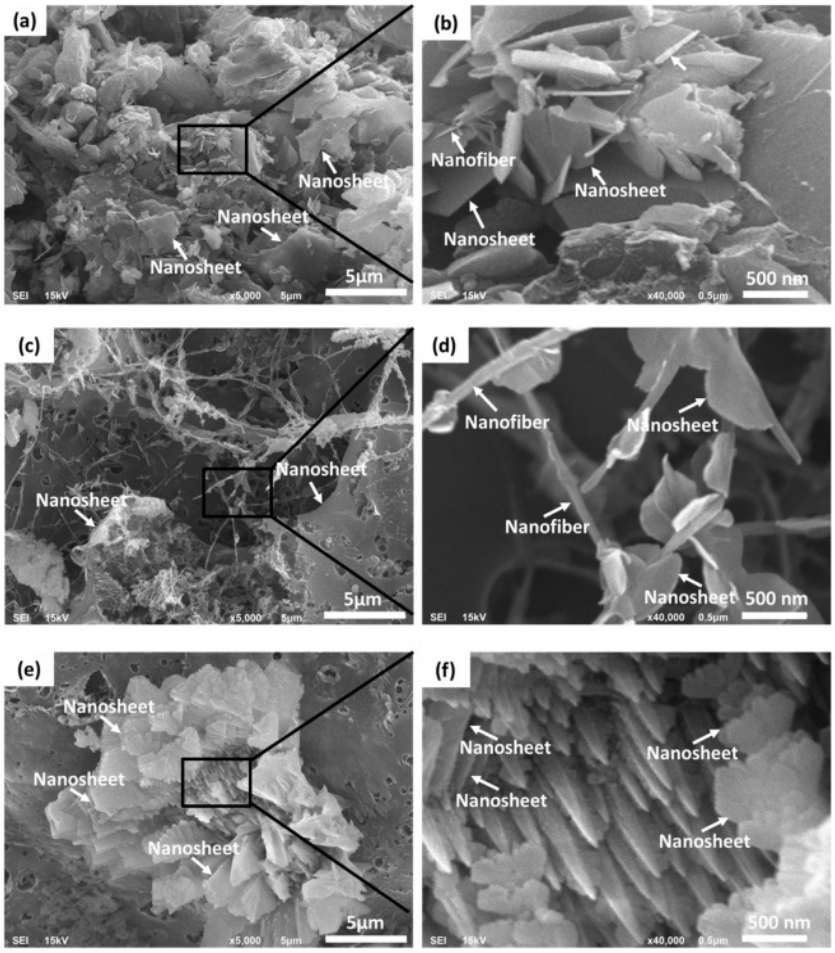

Fig. 3 – SEM micrograph of (a) ACS500, (b) enlarge of ACS500, (c) ACS600, (d) enlarge of ACS600, (e) ACS700, and (f) enlarge of ACS700.

well-connected pores and facilitates easier ion diffusion. The process of activation of high-temperature physical activation has a real effect, and the development of mesopores on the surface of the electrode is visible. Additionally, the abundance of porosity in nanosheets decorated by nanofibers has a high combination of micro- and mesoporous active sites for ions to form electric double layers, and channels to simplify the diffusion process and accelerate the ion rate transformation.

More importantly, thin and small like-flowers nanosheets are formed with a further addition of carbonization temperature (700 °C) as shown in Fig. 3e. The carbonization temperatures higher than 700 °C causes complete decomposition of cellulose and hemicellulose, reducing and eliminating fibers on the electrode surface. Furthermore, the composition of the reduced lignin forms a relatively smaller nanosheet [26]. Larger nanosheets formed previously are also degraded into comparatively smaller sheets [27]. Moreover, physical activation shows that mesopores are highly developed among these nanosheets, as indicated in Fig. 3f. This nanoscale structure is critical in providing active sites for ion diffusion and offering high specific surface areas on carbon. The unique nanostructure combination of activated carbon produced from pure biomass material (*Syzygium oleana* leaves) without other synthetic substances is an extraordinary achievement in the material surface. This has a major contribution in determining the ideal material for high-performance supercapacitor electrodes.

The porosity of activated carbon of *Syzygium oleana* leaves is determined by the N_2 adsorption and desorption. Fig. 4a shows the isotherms of all samples, including the combined characteristics of type I and type IV isotherms with a type H4 hysteresis loop at $P/P0 > 0.4$. The hysteresis loop varies according to the carbonization temperature, from 500 to 700 °C. The curve shows the presence of micropores and mesopores in the synthesized product [28]. The line observed in the low-pressure region indicates the presence of microporosity while the presences of a hysteresis loop in the high-pressure region shows the mesoporous structure. The isotherm curve at car-

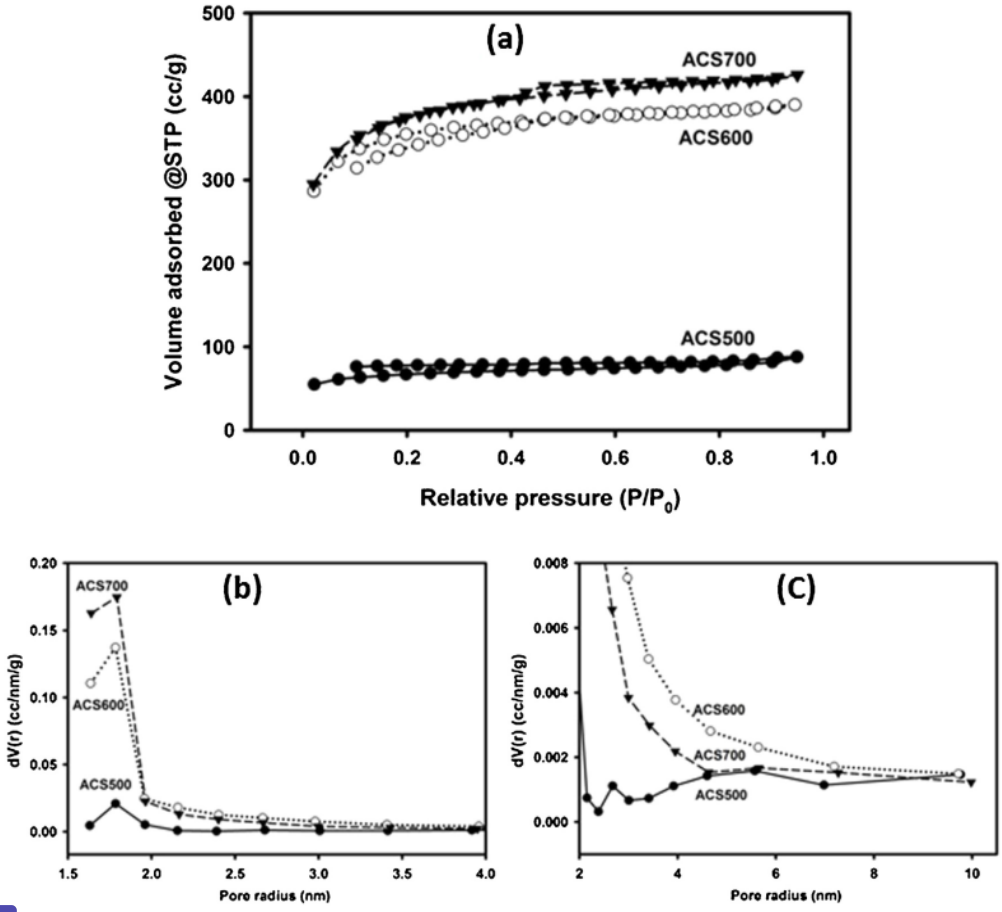

Fig. 4 – (a) N_2 gas adsorption/desorption of ACSs samples, (b), and (c) Pore sizes distribution of ACSs samples.

bonization temperatures of 500 °C and 600 °C for ACS500 and ACS600 samples shows an imperfect H4 type hysteresis curve. This is indicated by mesopores developing like ink bottles with narrow neck pore involving complex mechanisms. The capillary condensation from the pore tissue is blocked by narrowing the pores, slowing down the rate of desorption [29]. The higher addition to the 700 °C carbonization temperature for ACS700 sample causes the ink bottle pores to degrade and form an intact mesoporous. This leads to an ideal type IV hysteresis loop, as shown on the ACS700 isotherm curve.

Fig. 4b-c illustrates the pore size distribution of activated carbon prepared. All samples exhibit similar hierarchical porosity which contains small micropores of less than 2 nm and large mesopores of 2–10 nm. The ACS700 sample showed a predominance of smaller pores of more than 3 nm and was followed by ACS600 and ACS500. The number of developments of smaller pores allows the provision of high surface area and active sites for ion diffusion at the electrode/electrolyte interface. Also, the distribution is different at 2–10 nm, where ACS600 shows more pore combinations compared to ACS500 and ACS700. The phenomenon allows for a better pore distribution between micro-, meso-, and macropores. It supports the supply of more charge layers and expedites ion transfer at the porous carbon electrodes. The advantage of these properties increases the performance of double-layer supercapacitors [30]. Further information about specific surface areas and average pore diameters are shown in Table 1. The specific surface areas are 216 $m^2 g^{-1}$, 1137 $m^2 g^{-1}$, and 1218 $m^2 g^{-1}$ for ACS500, ACS600, and ACS700, respectively. Therefore, carbonization temperatures have successfully increased the specific surface area of activated carbon as well as total pore volume. Furthermore, the S_{mic}/S_{BET} value of ACS600 was larger than ACS500 and ACS700. This is revealed that a lower carbonization temperature could be easily inserted into the carbon layers to activate the carbon frameworks for enhancing the micropores area. However, as the carbonization temperature increased further corroding the wall of the micropores, and caused the broadening of pore size and the collapse of the pore structures, resulting in the decrease of the S_{mic}/S_{BET}. The carbonization temperature of 500 °C leads to an average pore diameter of 2.51 nm. Also, the addition of carbonization temperatures of 600 °C and 700 °C causes a reduction in the average pore diameter of 2.13 nm and 2.17 nm, respectively. From the above analysis, ACS600 has a high specific surface

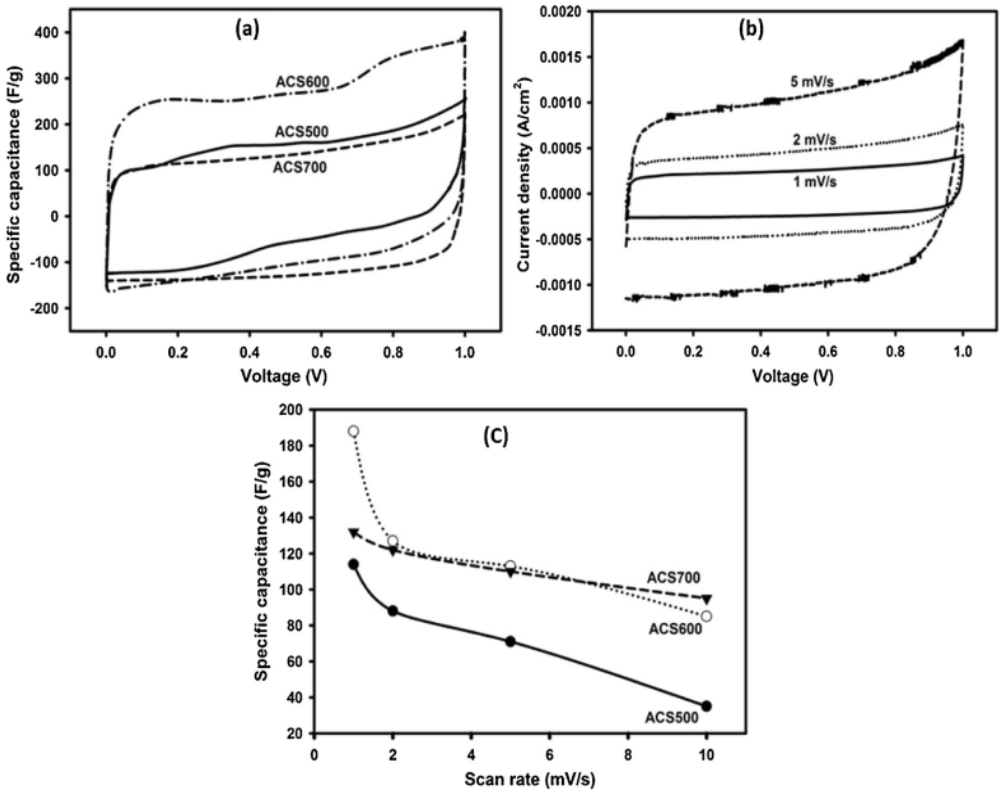

Fig. 5 – (a) CV curve of ACSs samples, (b) CV curve of ACS700 at different scan rate, and (c) specific capacitance vs scan rate of ACSs samples.

Table 1 – The specific surface area and average pores diameter of ACSs samples.

Samples	S_{BET} (m^2 g^{-1})	S_{micro} (m^2 g^{-1})	S_{meso}(m^2 g^{-1})	S_{mic}/S_{BET} (%)	V_{tot} (cm^3 g^{-1})	V_{micro} (cm^3 g^{-1})	V_{meso} (cm^3 g^{-1})	D_{aver} (nm)
ACS500	216.21	201.802	14.414	93.33	0.1361	0.1125	0.0236	2.51
ACS600	1137.61	1102.091	35.519	96.87	0.6051	0.5592	0.0459	2.13
ACS700	1218.41	1168.582	49.818	95.91	0.6606	0.5980	0.0626	2.17

area and a good pore combination (micro-, meso-, and macropores). This supports the application of materials prepared for high performance from supercapacitors.

The cyclic voltammetry was used to determine the performance of ACSs electrodes. Specific capacitance, energy density, and power density were determined from the cyclic voltammogram generated using a standard equations [31,32]. The electrochemical properties of the ACSs electrodes were evaluated using cyclic voltammetry with two electrode systems at 1.0 M H_2SO_4 electrolytes, as shown in Fig. 5a. All CV curves of ACSs based on the difference in carbonization temperature show a quasi-rectangular shape with different areas indicating distinct specific capacitance. The specific capacitance produced based on different carbonization temperatures for ACS500, ACS600, and ACS700 include 114 $F g^{-1}$, 188 F g^{-1}, and 132 F g^{-1}, respectively. Therefore, similarities were observed between the Specific capacitances, energy and power densities produced in this study, compared to previous reports, as shown in Table 2. The CV ACS500 and ACS600 curves show a clear redox peak and show a distorted rectangular shape, which indicates the behavior of the electrochemical double layer and capacitive pseudocapacitance. The presence of pseudo properties was indicated from the ZnO contents in the samples, as illustrated in the XRD analysis. The specific capacitance of ACS600 sample was significantly higher than those of ACS500, and ACS700, despite the not higher in specific surface area due to combination structure of nanosheet and nanofiber contribute to the accessibility of suitable active surface area, intercalation/de-intercalation reaction easily occurred in H_2SO_4 electrolyte thereby increasing the double layer as well as pseudocapacitance [33]. In addition, the higher S_{mic}/S_{BET} provide three-dimensional pore connections for ion diffusion into electrode/ electrolyte interface [34]. This produces high capacitive properties with maximum energy and power densities of 26 Wh kg^{-1} and 94 W kg^{-1}. Compared to ACS500 and ACS600, the CV ACS700 curve shows

Table 2 – The comparison of specific capacitance, energy density and power density of different biomass wastes.

Biomass sources	Preparation methods	C_{sp} (F g^{-1})	E (Wh kg^{-1})	P (W kg^{-1})	Ref
Butnea Monosperma flower pollen	One-step thermal activation process	130	42	19k	[36]
Rice straw	Hydrothermal treatment	337	9.31	500	[37]
Tobacco waste	N_2-carbonization	148	2.66	51	[38]
Peanut shell	One-step microwave-assisted $ZnCl_2$ activation	184	4.94	740	[39]
Cauliflower	Two-stage thermochemical	311	20.5	448.8	[32]
Corncob residue	One-step activation process	314	6.8	17	[40]
Oil palm empty Fruit bunches	N_2-carbonization and CO_2-activation	150	4.297	173	[41]
Soybean shell	Hydrothermal treatment	301	8.1	21.9	[42]
Syzygium oleana leaves	One-stage integrated pyrolysis	188	26	96	This work

a quasi-rectangular shape without any pseudocapacitance effect, indicating that the sample has an ideal behavior of electrochemical double layers [35]. Increasing the carbonization temperature to 700 °C reduces and removes ZnO, enhancing the charge double layer properties. This is also contributed by $ZnCl_2$ activation, which develops pure nanosheet structure with micro- and mesoporous properties at high temperatures and optimizes transport channels for electrolytes. As the temperature continues to rise, heteroatoms decrease, and the microstructure is extended further. The structure of small nanosheets with micro-, meso-, and macropores on the surface of carbon electrodes has almost the same effect on the sample.

The CV curve for ACS700 is shown in Fig. 5b at the scan rate of 1, 2, 5, and 10 mV s^{-1}. It retains a rectangular shape at different scan rates, showing a superior electrode charge/discharge and excellent capacitive and reversibility characteristics. Fig. 5c shows the specific capacitance for all samples at different scanning rates. The specific capacitance decreases with increasing scan rate. The specific capacitance of ACS500 and ACS600 decreases more significantly compared to ACS700 by increasing the scanning rate. This result can be attributed to the unique micro-mesoporous structure of ACS700. Micropores provide abundant surface active sites for charge adsorption, fast ionic transport channels in the mesoporous, and smaller nanosheets which provide a relatively short diffusion distance of electrolyte ions from the mesoporous to the micropore. Therefore, ACS700 electrodes are considered to be more stable compared to ACS600 and ACS500. However, the highest specific capacitance is found on ACS600.

4. Conclusion

The porous activated carbon nanosheets were successfully prepared using *Syzygium oleana leaves* wastes as a precursor. A *Syzygium oleana* leaves a potential pure biomass material for a high density of activated carbon nanosheets without the template method, composite, and other synthetic materials. Outstandingly, one-stage integrated pyrolysis was used to prepare porous carbon nanosheets. This was meant to improve the specific surface area and suitable pore size distribution for high rate ion transfer in the electrode/electrolyte interface. The different carbonization temperatures show unique nanomaterial surface morphology. The carbonization temperature of 500 °C and 600 °C produces nanosheet morphology emblazoned by nanofibers. In contrast, a temperature of 700 °C produces high-density like-flower nanosheets. This unique nanomaterial allows hierarchical mesoporous active sites to form electric double layers and diffusion channels to simplify the entire process and accelerate the ion rate transformation. Furthermore, the ACS600 has the best electrochemical properties in a two-electrode system with an increase in specific capacitance from 114 F g^{-1} to 188 F g^{-1}, resulting to a high energy and power densities of 26 Wh kg^{-1} and 96 W kg^{-1}. However, ACS700 can be considered to be more stable in different scan rates of 1 mV s^{-1}, 2 mV s^{-1}, 5 mV s^{-1}, and 10 mV s^{-1}. Therefore, the one-stage integrated pyrolysis method maximizes the great potential of *Syzygium oleana* leaves waste as a raw material for porous carbon nanosheets to boosting supercapacitor performance.

Declaration of interests

The authors declare that they have no known competing financial interests or personal relationships that could have appeared to influence the work reported in this paper.

Acknowledgement

This study was funded by DRPM Kemenristek-Dikti through second year Project of PD (396/UN.19.5.1.3/PT.01.03/2020) with the title "High-density micro-and nano carbon fiber made from biomass based materials for supercapacitor electrodes".

REFERENCES

[1] Chen M, Zhou S, Zhu Y, Sun Y, Zeng G, Yang C, et al. Toxicity of carbon nanomaterials to plants, animals and microbes: recent progress from 2015-present. Chemosphere 2018;206:255–64, http://dx.doi.org/10.1016/j.chemosphere.2018.05.020.

[2] Jiang BP, Zhou B, Lin Z, Liang H, Shen XC. Recent advances in carbon nanomaterials for Cancer phototherapy. Chem - A Eur J 2019;25:3993–4004, http://dx.doi.org/10.1002/chem.201804383.

[3] Li J, Hu H, Li H, Yao C. Recent developments in electrochemical sensors based on nanomaterials for determining glucose and its byproduct H2O2. J Mater Sci 2017;52:10455–69, http://dx.doi.org/10.1007/s10853-017-1221-4.

[4] Yan D, Lei B, Chen B, Wu XJ, Liu Z, Li N, et al. Synthesis of high-quality lanthanide oxybromides nanocrystals with single-source precursor for promising applications in cancer

cells imaging. Appl Mater Today 2015;1:20–6, http://dx.doi.org/10.1016/j.apmt.2015.06.001.
[5] Max Lu GQ, Qiao S, Nair S. Special Issue on nanomaterials for catalysis and electrochemical processes. Chem Eng Sci 2019;194:1, http://dx.doi.org/10.1016/j.ces.2018.10.027.
[6] Lee J, Lee K, Park SS. Environmentally friendly preparation of nanoparticle-decorated carbon nanotube or graphene hybrid structures and their potential applications. J Mater Sci 2016;51:2761–70, http://dx.doi.org/10.1007/s10853-015-9581-0.
[7] Huo S, Liu M, Wu L, Liu M, Xu M, Ni W, et al. Synthesis of ultrathin and hierarchically porous carbon nanosheets based on interlayer-confined inorganic/organic coordination for high performance supercapacitors. J Power Sources 2019;414:383–92, http://dx.doi.org/10.1016/j.jpowsour.2019.01.028.
[8] Dhara K, Mahapatra DR. Recent advances in electrochemical nonenzymatic hydrogen peroxide sensors based on nanomaterials: a review. J Mater Sci 2019;54:12319–57, http://dx.doi.org/10.1007/s10853-019-03750-y.
[9] Vikrant K, Bhardwaj N, Bhardwaj SK, Kim K, Deep A. Biomaterials Nanomaterials as efficient platforms for sensing DNA. Biomaterials 2019;214:1–18, http://dx.doi.org/10.1016/j.biomaterials.2019.05.026.
[10] Wildfire C, Çiftyürek E, Sabolsky K, Sabolsky EM. Investigation of doped-gadolinium zirconate nanomaterials for high-temperature hydrogen sensor applications. J Mater Sci 2014;49:4735–50, http://dx.doi.org/10.1007/s10853-014-8173-8.
[11] Kim J, Won H, Min S, Jae J, Park Y. Overview of the recent advances in lignocellulose liquefaction for producing biofuels, bio-based materials and chemicals. Bioresour Technol 2019;279:373–84, http://dx.doi.org/10.1016/j.biortech.2019.01.055.
[12] Ren S, Yang W, Li Y. Synthetic biopigment supercapacitors. ACS Appl Mater Interfaces 2019;11:30360–7, http://dx.doi.org/10.1021/acsami.9b10956.
[13] Jose J, Thomas V, Vinod V, Abraham R, Abraham S. Nanocellulose based functional materials for supercapacitor applications. J Sci Adv Mater Devices 2019;4:333–40, http://dx.doi.org/10.1016/j.jsamd.2019.06.003.
[14] Poonam, Sharma K, Arora A, Tripathi SK. Review of supercapacitors: materials and devices. J Energy Storage 2019;21:801–25, http://dx.doi.org/10.1016/j.est.2019.01.010.
[15] Liu F, Wang Z, Zhang H, Jin L, Chu X, Gu B, et al. Nitrogen, oxygen and sulfur co-doped hierarchical porous carbons toward high-performance supercapacitors by direct pyrolysis of kraft lignin. Carbon N Y 2019;149:105–16, http://dx.doi.org/10.1016/j.carbon.2019.04.023.
[16] Sun Y, Guo S, Li W, Pan J, Fernandez C, Arumugam R, et al. A green and template-free synthesis process of superior carbon material with ellipsoidal structure as enhanced material for supercapacitors. J Power Sources 2018;405:80–8, http://dx.doi.org/10.1016/j.jpowsour.2018.10.034.
[17] Dehkhoda AM, Gyenge E, Ellis N. A novel method to tailor the porous structure of KOH-activated biochar and its application in capacitive deionization and energy storage. Biomass Bioenergy 2016;87:107–21, http://dx.doi.org/10.1016/j.biombioe.2016.02.023.
[18] Thomas P, Lai CW, Bin Johan MR. Recent developments in biomass-derived carbon as a potential sustainable material for super-capacitor-based energy storage and environmental applications. J Anal Appl Pyrolysis 2019;140:54–85, http://dx.doi.org/10.1016/j.jaap.2019.03.021.
[19] Taer E, Sumantre MAA, Taslim R, Dahlan D, Deraman M. Eggs shell membrane as natural separator for supercapacitor applications. Adv Mater Res 2014;896:66–9, http://dx.doi.org/10.4028/www.scientific.net/AMR.896.66.
[20] Khan TA, Saud AS, Jamari SS, Rahim MHA, Park JW, Kim HJ. Hydrothermal carbonization of lignocellulosic biomass for carbon rich material preparation: a review. Biomass Bioenergy 2019;130:105384, http://dx.doi.org/10.1016/j.biombioe.2019.105384.
[21] Taer E, Apriwandi A, Taslim R, Malik U, Usman Z. Single step carbonization-activation of durian shells for producing activated carbon monolith electrodes. Int J Electrochem Sci 2019;14:1318–30, http://dx.doi.org/10.20964/2019.02.67.
[22] Yang V, Senthil RA, Pan J, Khan A, Osman S, Wang L, et al. Highly ordered hierarchical porous carbon derived from biomass waste mangosteen peel as superior cathode material for high performance supercapacitor. J Electroanal Chem (Lausanne) 2019:113616, http://dx.doi.org/10.1016/j.jelechem.2019.113616.
[23] Boujibar O, Ghosh A, Achak O, Chafik T, Ghamouss F. A high energy storage supercapacitor based on nanoporous activated carbon electrode made from Argan shells with excellent ion transport in aqueous and non-aqueous electrolytes. J Energy Storage 2019;26:100958, http://dx.doi.org/10.1016/j.est.2019.100958.
[24] Palisoc S, Dungo JM, Natividad M. Low-cost supercapacitor based on multi-walled carbon nanotubes and activated carbon derived from Moringa oleifera fruit shells. Heliyon 2020;6:e03202, http://dx.doi.org/10.1016/j.heliyon.2020.e03202.
[25] Cai Y, Luo Y, Dong H, Zhao X, Xiao Y, Liang Y, et al. Hierarchically porous carbon nanosheets derived from Moringa oleifera stems as electrode material for high-performance electric double-layer capacitors. J Power Sources 2017;353:260–9, http://dx.doi.org/10.1016/j.jpowsour.2017.04.021.
[26] Xie A, Dai J, Chen Y, Liu N, Ge W, Ma P, et al. NaCl-template assisted preparation of porous carbon nanosheets started from lignin for efficient removal of tetracycline. Adv Powder Technol 2019;30:170–9, http://dx.doi.org/10.1016/j.apt.2018.10.020.
[27] Wang Y, Li W, Zhang L, Zhang X, Tan B, Hao J, et al. Amorphous cobalt hydrogen phosphate nanosheets with remarkable electrochemical performances as advanced electrode for supercapacitors. J Power Sources 2020;449:227487, http://dx.doi.org/10.1016/j.jpowsour.2019.227487.
[28] Sing KSW. Reporting physisorption data for gas/solid systems with special reference to the determination of surface area and porosity. Pure Appl Chem 1982;54:2201–18, http://dx.doi.org/10.1351/pac198254112201.
[29] Ayinla RT, Dennis JO, Zaid HM, Sanusi YK, Usman F, Adebayo LL. A review of technical advances of recent palm bio-waste conversion to activated carbon for energy storage. J Clean Prod 2019;229:1427–42, http://dx.doi.org/10.1016/j.jclepro.2019.04.116.
[30] Miller EE, Hua Y, Tezel FH. Materials for energy storage: review of electrode materials and methods of increasing capacitance for supercapacitors. J Energy Storage 2018;20:30–40, http://dx.doi.org/10.1016/j.est.2018.08.009.
[31] Liao MD, Peng C, Hou SP, Chen J, Zeng XG, Wang HL, et al. Large-scale synthesis of nitrogen-doped activated carbon fibers with high specific surface area for high-performance supercapacitors. Energy Technol 2020;8:1901477, http://dx.doi.org/10.1002/ente.201901477.
[32] Men B, Guo P, Sun Y, Tang Y, Chen Y, Pan J, et al. High-performance nitrogen-doped hierarchical porous carbon derived from cauliflower for advanced supercapacitors. J Mater Sci 2019;54:2446–57, http://dx.doi.org/10.1007/s10853-018-2979-8.
[33] Misnon II, Aziz RA, Zain NKM, Vidhyadharan B, Krishnan SG, Jose R. High performance MnO2 nanoflower electrode and

the relationship between solvated ion size and specific capacitance in highly conductive electrolytes. Mater Res Bull 2014;57:221–30, http://dx.doi.org/10.1016/j.materresbull.2014.05.044.
[34] Wang Q, Liu F, Jin Z, Qiao X, Huang H, Chu X, et al. Hierarchically divacancy defect building dual-activated porous carbon fibers for high-performance energy-storage devices; 2020. p. 1–8, http://dx.doi.org/10.1002/adfm.202002580, 2002580.
[35] Taer E. Preparation of mission grass flower-based activated carbon monolith electrode for supercapacitor application. Int J Electrochem Sci 2019;14:7317–31, http://dx.doi.org/10.20964/2019.08.82.
[36] Ahmed S, Ahmed A, Rafat M. Investigation on activated carbon derived from biomass Butnea monosperma and its application as a high performance supercapacitor electrode. J Energy Storage 2019;26:100988, http://dx.doi.org/10.1016/j.est.2019.100988.
[37] Liu S, Zhao Y, Zhang B, Xia H, Zhou J, Xie W, et al. Nano-micro carbon spheres anchored on porous carbon derived from dual-biomass as high rate performance supercapacitor electrodes. J Power Sources 2018;381:116–26, http://dx.doi.org/10.1016/j.jpowsour.2018.02.014.
[38] Chen H, Guo YC, Wang F, Wang G, Qi PR, Guo XH, et al. An activated carbon derived from tobacco waste for use as a supercapacitor electrode material. New Carbon Mater 2017;32:592–9, http://dx.doi.org/10.1016/S1872-5805(17)60140-9.
[39] He X, Li R, Han J, Yu M, Wu M. Facile preparation of mesoporous carbons for supercapacitors by one-step microwave-assisted $ZnCl_2$ activation. Mater Lett 2013;94:158–60, http://dx.doi.org/10.1016/j.matlet.2012.12.031.
[40] Qu W, Xu Y, Lu A, Zhang X, Li W. Converting biowaste corncob residue into high value added porous carbon for supercapacitor electrodes. Bioresour Technol 2015, http://dx.doi.org/10.1016/j.biortech.2015.04.005.
[41] Farma R, Deraman M, Awitdrus A, Talib IA, Taer E, Basri NH, et al. Preparation of highly porous binderless activated carbon electrodes from fibres of oil palm empty fruit bunches for application in supercapacitors. Bioresour Technol 2013;132:254–61, http://dx.doi.org/10.1016/j.biortech.2013.01.044.
[42] Wu Y, Cao JP, Zhao XY, Zhuang QQ, Zhou Z, Zhao M, et al. Sustainable Porous Carbon with High Specific Surface Area from Soybean Shell via Hydrothermal Carbonization with H_3PO_4 for Electric Double-Layer Capacitor Applications. Energy Technol 2020;8:1901103, http://dx.doi.org/10.1002/ente.201901103.

Conversion Syzygium oleana leaves biomass waste to porous activated carbon nanosheet for boosting supercapacitor performances

ORIGINALITY REPORT

19%	8%	18%	4%
SIMILARITY INDEX	INTERNET SOURCES	PUBLICATIONS	STUDENT PAPERS

PRIMARY SOURCES

1	Xiao-Qiang Lin, Ning Yang, Qiu-Feng Lü, Rui Liu. "Self-Nitrogen-Doped Porous Biocarbon from Watermelon Rind: A High-Performance Supercapacitor Electrode and Its Improved Electrochemical Performance Using Redox Additive Electrolyte", Energy Technology, 2019 Publication	2%
2	Erman Taer, Martauli Sihombing, Rika Taslim, Agustino, Apriwandi. "Bamboo-Based Activated Carbon as Binder-Free Electrode of Supercapacitor Application", Journal of Physics: Conference Series, 2020 Publication	1%
3	A.A. Menazea, A.M. Ismail, I.S. Elashmawi. "The role of Li4Ti5O12 nanoparticles on enhancement the performance of PVDF/PVK blend for lithium-ion batteries", Journal of Materials Research and Technology, 2020 Publication	1%

4	acris.aalto.fi Internet Source	1%
5	Sultan Ahmed, Ahsan Ahmed, M. Rafat. "Investigation on activated carbon derived from biomass Butnea monosperma and its application as a high performance supercapacitor electrode", Journal of Energy Storage, 2019 Publication	1%
6	Submitted to Universidade Estadual de Campinas Student Paper	1%
7	www.jmrt.com.br Internet Source	1%
8	etd.library.vanderbilt.edu Internet Source	1%
9	Jung-Jie Huang, Yu-Lee Hsueh, Yu-Xuan Zhang. "Silver nanowire doped active carbon thin film electrode by ultrasonic spray coating for high performance supercapacitor", Surface and Coatings Technology, 2018 Publication	1%
10	Amir Mehdi Dehkhoda, Előd Gyenge, Naoko Ellis. "A novel method to tailor the porous structure of KOH-activated biochar and its application in capacitive deionization and energy	1%

storage", Biomass and Bioenergy, 2016
Publication

11	Erman Taer, Friska Febriyanti, Widya Sinta Mustika, Rika Taslim, Agustino Agustino, Apriwandi Apriwandi. "Enhancing the performance of supercapacitor electrode from chemical activation of carbon nanofibers derived Areca catechu husk via one-stage integrated pyrolysis", Carbon Letters, 2020 Publication	1%
12	electrochemsci.org Internet Source	1%
13	Urbano Díaz, Teresa García, Alexandra Velty, Avelino Corma. "Synthesis and Catalytic Properties of Hybrid Mesoporous Materials Assembled from Polyhedral and Bridged Silsesquioxane Monomers", Chemistry - A European Journal, 2012 Publication	1%
14	Lin-Lin Zhang, Huan-Huan Li, Yan-Hong Shi, Chao-Ying Fan, Xing-Long Wu, Hai-Feng Wang, Hai-Zhu Sun, Jing-Ping Zhang. "A Novel Layered Sedimentary Rocks Structure of the Oxygen-Enriched Carbon for Ultrahigh-Rate-Performance Supercapacitors", ACS Applied Materials & Interfaces, 2016 Publication	<1%

15	pubs.acs.org Internet Source	<1%
16	Rong Shao, Jin Niu, Jingjing Liang, Mengyue Liu, Zhengping Zhang, Meiling Dou, Yaqin Huang, Feng Wang. "Mesopore- and Macropore-Dominant Nitrogen-Doped Hierarchically Porous Carbons for High-Energy and Ultrafast Supercapacitors in Non-Aqueous Electrolytes", ACS Applied Materials & Interfaces, 2017 Publication	<1%
17	Submitted to Indian Institute of Space Science and Technology Student Paper	<1%
18	Elizabeth Esther Miller, Ye Hua, F. Handan Tezel. "Materials for energy storage: Review of electrode materials and methods of increasing capacitance for supercapacitors", Journal of Energy Storage, 2018 Publication	<1%
19	Submitted to VIT University Student Paper	<1%
20	Basri, N.H., M. Deraman, S. Kanwal, I.A. Talib, J.G. Manjunatha, A.A. Aziz, and R. Farma. "Supercapacitors using binderless composite monolith electrodes from carbon nanotubes and	<1%

pre-carbonized biomass residues", Biomass and Bioenergy, 2013.
Publication

21	Mohd Nor, Najah Syahirah, Mohamad Deraman, Ramli Omar, Awitdrus, Rakhmawati Farma, Nur Hamizah Basri, Besek Nurdiana Mohd Dolah, Nurul Fatin Mamat, Baharudin Yatim, and Mohd Norizam Md Daud. "Influence of gamma irradiation exposure on the performance of supercapacitor electrodes made from oil palm empty fruit bunches", Energy, 2015. Publication	<1%
22	www.uts.edu.au Internet Source	<1%
23	www.scielo.cl Internet Source	<1%
24	Zan Gao, Yunya Zhang, Ningning Song, Xiaodong Li. "Biomass-derived renewable carbon materials for electrochemical energy storage", Materials Research Letters, 2016 Publication	<1%
25	Yu Wang, Ying Zhu, Hailiang Chu, Shujun Qiu et al. "Porous Carbons Derived from Ginkgo Shell Used for High-Performance Supercapacitors", Nanoarchitectonics, 2020 Publication	<1%

---

www.degruyter.com

26	Internet Source	<1%
27	hal.univ-lorraine.fr Internet Source	<1%
28	Hui Chen, Yan-chuan Guo, Fu Wang, Gang Wang, Pei-rong Qi, Xu-hong Guo, Bin Dai, Feng Yu. "An activated carbon derived from tobacco waste for use as a supercapacitor electrode material", New Carbon Materials, 2017 Publication	<1%
29	eprints.lib.hokudai.ac.jp Internet Source	<1%
30	HeMing Luo, YanZheng Chen, Bo Mu, YuanJie Fu, Xia Zhao, JianQiang Zhang. "Preparation and electrochemical performance of attapulgite/citric acid template carbon electrode materials", Journal of Applied Electrochemistry, 2016 Publication	<1%
31	R. Taslim, T.R. Dewi, E. Taer, A. Apriwandi, A. Agustino, R. N. Setiadi. "Effect of physical activation time on the preparation of carbon electrodes from pineapple crown waste for supercapacitor application", Journal of Physics: Conference Series, 2018 Publication	<1%

32	Yufeng Zhao, Wei Ran, Jing He, Yanfang Song, Chunming Zhang, Ding-Bang Xiong, Faming Gao, Jinsong Wu, Yongyao Xia. "Oxygen-Rich Hierarchical Porous Carbon Derived from Artemia Cyst Shells with Superior Electrochemical Performance", ACS Applied Materials & Interfaces, 2015 Publication	<1%
33	P. D. More, P. R. Jadhav, A. A. Ghanwat, I. A. Dhole, Y. H. Navale, V. B. Patil. "Spray synthesized hydrophobic α-Fe2O3 thin film electrodes for supercapacitor application", Journal of Materials Science: Materials in Electronics, 2017 Publication	<1%
34	Shaobo Liu, Yang Zhao, Baihui Zhang, Hui Xia, Jianfei Zhou, Wenke Xie, Hongjian Li. "Nano-micro carbon spheres anchored on porous carbon derived from dual-biomass as high rate performance supercapacitor electrodes", Journal of Power Sources, 2018 Publication	<1%
35	Misnon, Izan Izwan, Radhiyah Abd Aziz, Nurul Khairiyyah Mohd Zain, Baiju Vidhyadharan, Syam G. Krishnan, and Rajan Jose. "High performance MnO2 nanoflower electrode and the relationship between solvated ion size and	<1%

specific capacitance in highly conductive electrolytes", Materials Research Bulletin, 2014.
Publication

---

36 Wang, Keliang, Yuhe Cao, Xiaomin Wang, Qihua Fan, William Gibbons, Tylor Johnson, Bing Luo, and Zhengrong Gu. "Pyrolytic cyanobacteria derived activated carbon as high performance electrode in symmetric supercapacitor", Energy, 2016. <1%
Publication

---

37 Huaqing Xuan, Gaoxin Lin, Fan Wang, Jiyang Liu, Xiaoping Dong, Fengna Xi. "Preparation of biomass-activated porous carbons derived from torreya grandis shell for high-performance supercapacitor", Journal of Solid State Electrochemistry, 2017 <1%
Publication

---

38 Rashma Chaudhary, Subrata Maji, Rekha Goswami Shrestha, Ram Lal Shrestha, Timila Shrestha, Katsuhiko Ariga, Lok Kumar Shrestha. "Jackfruit Seed-Derived Nanoporous Carbons as the Electrode Material for Supercapacitors", C, 2020 <1%
Publication

---

39 Suresh Kumar, Rahul R. Nair, Premlal B. Pillai, Satyendra Nath Gupta, M. A. R. Iyengar, A. K. Sood. " Graphene Oxide–MnFe O Magnetic <1%

Nanohybrids for Efficient Removal of Lead and Arsenic from Water ", ACS Applied Materials & Interfaces, 2014
Publication

40	www.jmst.org Internet Source	<1%
41	eprints.whiterose.ac.uk Internet Source	<1%
42	vtechworks.lib.vt.edu Internet Source	<1%
43	Zan Peng, Xiaojuan Liu, Wei Zhang, Zhuotong Zeng et al. "Advances in the application, toxicity and degradation of carbon nanomaterials in environment: A review", Environment International, 2020 Publication	<1%
44	Agustino, Awitdrus, Amun Amri, Rika Taslim, Erman Taer. "The Physical and Electrochemical Properties of Activated Carbon Electrode Derived from Pineapple Leaf Waste for Supercapacitor Applications", Journal of Physics: Conference Series, 2020 Publication	<1%
45	Nanostructure Science and Technology, 2016. Publication	<1%
46	Hongcai Gao, Fei Xiao, Chi Bun Ching, Hongwei	

	Duan. " Flexible All-Solid-State Asymmetric Supercapacitors Based on Free-Standing Carbon Nanotube/Graphene and Mn O Nanoparticle/Graphene Paper Electrodes ", ACS Applied Materials & Interfaces, 2012 Publication	<1%
47	Jie Cai, Haitao Niu, Zhenyu Li, Yong Du, Pavel Cizek, Zongli Xie, Hanguo Xiong, Tong Lin. "High-Performance Supercapacitor Electrode Materials from Cellulose-Derived Carbon Nanofibers", ACS Applied Materials & Interfaces, 2015 Publication	<1%
48	Arnaud Gigot, Marco Fontana, Mara Serrapede, Micaela Castellino et al. " Mixed 1T–2H Phase MoS /Reduced Graphene Oxide as Active Electrode for Enhanced Supercapacitive Performance ", ACS Applied Materials & Interfaces, 2016 Publication	<1%
49	Linlin Xing, Xun Chen, Zhixiang Tan, Manzhou Chi et al. "Synthesis of Porous Carbon Material with Suitable Graphitization Strength for High Electrochemical Capacitors", ACS Sustainable Chemistry & Engineering, 2019 Publication	<1%
50	Yang Liu, Zijun Shi, Yanfang Gao, Weidan An,	<1%

Zhenzhu Cao, Jinrong Liu. "Biomass-Swelling Assisted Synthesis of Hierarchical Porous Carbon Fibers for Supercapacitor Electrodes", ACS Applied Materials & Interfaces, 2016
Publication

---

51 Abdelhakim Elmouwahidi, Esther Bailón-García, Agustín F. Pérez-Cadenas, Francisco J. Maldonado-Hódar et al. "Activated carbons from KOH and H 3 PO 4 -activation of olive residues and its application as supercapacitor electrodes", Electrochimica Acta, 2017 <1%
Publication

---

52 "Characterization of Minerals, Metals, and Materials 2020", Springer Science and Business Media LLC, 2020 <1%
Publication

Exclude quotes	On	Exclude matches	Off
Exclude bibliography	On		